THE JOURNAL OF PHYSICAL CHEMISTRY C

Article

Cite This: J. Phys. Chem. C 2018, 122, 27745−27753

pubs.acs.org/JPCC

Effect of Edge Charges on Stability and Aggregation of $Ti_3C_2T_z$ MXene Colloidal Suspensions

Varun Natu, Maxim Sokol, Louisiane Verger, and Michel W. Barsoum*

Department of Materials Science and Engineering, Drexel University, Philadelphia, Pennsylvania 19104, United States

Supporting Information

ABSTRACT: Herein, the stabilities of aqueous $Ti_3C_2T_z$ (MXene) colloidal suspensions were studied as a function of pH and sodium chloride concentrations using ζ-potential and dynamic light scattering measurements. Complete sedimentation was observed when the pH was changed to 5 or 10. In the low pH regime, protons saturate the surface functional groups, rendering the ζ-potential less negative that, in turn, leads to aggregation. In the high pH regime, the ζ-potential remained constant up to a pH of almost 12. As the molarity of NaCl increases from 0 to 0.04, the ζ-potential goes from −35 to −22.5 mV. At a molarity of 0.02, sedimentation was observed. When the pH or NaCl concentration is high, sedimentation occurred, presumably, because of a reduction in the double-layer thickness. In all cases, the sediment comprised crumpled $Ti_3C_2T_z$ flakes. After adding charged nanoparticles to the colloidal suspension, at neutral pH, subsequent transmission electron microscope micrographs showed that the negative gold nanoparticles preferred the edges, whereas the positive ones preferred the surfaces. The charge differences between the edges and faces open opportunities for direct edge or face-specific organic functionalizations, similar to work done on other two-dimensional materials.

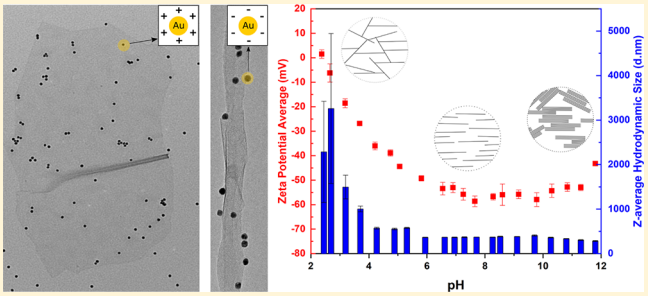

1. INTRODUCTION

Naguib et al. coined the term MXene when they first discovered the two dimenstional, 2D, layered transition metal carbide $Ti_3C_2T_z$ in 2011.[1] MXenes are generally produced by etching out the A layer from the MAX phases[1−4] or non-MAX-layered materials[5−7] using hydrofluoric acid or a combination of alkali fluoride salts and hydrochloric acid (HCl).[8] The MAX phases are layered ternary, metal carbides, and/or nitrides that have a general formula of $M_{n+1}AX_n$, where n is between 1 and 3, M stands for an early transition metal, A stands mostly for a group 13 or 14 element, and X for carbon or nitrogen.[8] The −ene suffix was added to MXene to make the connection to graphene with its good electrical conductivity.[9]

Upon etching, the MAX A layers—most often Al—are replaced by various functional groups such as −OH (hydroxyl), −O (oxygen), and −F (fluorine) that are, in turn, attached to the $M_{n+1}X_n$ surface, rendering them negative at neutral pH.[10−15]

Research on MXenes has exploded recently for many reasons. Arguably, the ease with which large quantities of relatively pure, aqueous, stable colloidal suspensions can be produced is one of the many advantages of working with MXenes that has rendered them so popular. But to date, the underlying reasons for the stability of these colloidal suspensions have not been explored in any systematic way. Maleski et al. carried out a detailed study on the stability of $Ti_3C_2T_z$ suspensions in different solvents and found that polar solvents are the most effective in producing stable colloids.[16] They proposed that the polar terminations on the $Ti_3C_2T_z$ sheets interact with polar solvents, that render the colloids stable.[16] The same group compared the hydrodynamic sizes obtained by dynamic light scattering (DLS) to those obtained by imaging, in a scanning electron microscope (SEM) and a transmission electron microscope (TEM) $Ti_3C_2T_z$ flakes and found the values obtained by the different techniques to be in good agreement with one another.[17] Akuzum et al. tested the rheological properties of $Ti_3C_2T_z$ colloids and found a viscoelastic component even at lower concentrations (<0.20 mg/mL) and attributed it to the high surface charge of individual $Ti_3C_2T_z$ sheets.[18] Prior to this work, the ζ-potential vs pH curves have been reported for various MXenes.[11,19,20] In all cases, the ζ-potential was found to increase rapidly with decreasing pH, but seems to be more or less constant with increasing pH. The reason for this asymmetry has, as far as we are aware, not been studied in detail.

Work done by Ghidiu et al. showed that the ion-exchange and hydration behaviors of $Ti_3C_2T_z$ multilayers, are similar to those of some clays.[8,21] This important insight is reinforced in this work. It is therefore useful to briefly summarize the aggregation behavior of clay colloids and the mechanisms involved. Schofield and Samson found that the stability of kaolinite clay colloid was pH sensitive and that flocculation

Received: September 10, 2018
Revised: October 27, 2018
Published: November 9, 2018

DOI: 10.1021/acs.jpcc.8b08860
J. Phys. Chem. C 2018, 122, 27745−27753

occurs in both acidic and basic media. Furthermore, they found that the addition of salts like NaCl, magnesium chloride ($MgCl_2$), among others, also led to aggregation. Rheological studies of pH or salt-induced aggregates of clay showed distinctly different behaviors. On the one hand, aggregates formed by the addition of a base or a salt resulted in a majority of face−face interactions between the clay sheets. On the other hand, the aggregates formed by the addition of an acid showed a higher degree of edge−face interactions. This difference in behavior was attributed to the positive charges on the edges of the clay sheets at low pH, which led to an electrostatic interaction between the positively charged edges and negatively charged surfaces. Conversely, at high pH, the −OH groups on the edges are deprotonated to $-O^-$, giving the edges a negative charge, thereby rendering edge−face interactions repulsive.[22,23]

By mixing a colloid of negatively charged gold nanoparticles (Au NPs) and kaolinite clay, Thießen, in 1947, was the first to report direct evidence for positive edge charges on kaolinite flakes. The images captured using a transmission electron microscope (TEM) clearly showed the negatively charged gold particles aligned around the edges of the clay nanosheets, whereas the positively charged gold nanoparticles covered the entire surface.[24] This was later shown to be true for other types of clays like montmorillonite, laponite, and so on.[25−28]

Apart from clays, aggregation is observed in other platelike particles as well. Pavlovic et al. showed that in layered double hydroxides, which have positively charged surfaces, anions, and not cations, are responsible for the aggregation.[29] Rouster et al. in their study of titania nanosheets studied the effect of pH and salt concentration simultaneously on aggregation. Interestingly, they found that above point of zero charge (PZC), the sheets were positively charged and anions were responsible for aggregation; below the PZC, the sheets were negatively charged and cations caused aggregation. Therefore, the effect of co-ions (ions that help maintain the colloidal stability) and counter ions (ions that cause aggregation) is pH dependent, and their roles are switched depending on the surface charge.[30] Graphene oxide (GO) sheets were shown to have carboxylic acid groups at their edges, whereas the surfaces were terminated mainly by hydroxyl groups. Wu et al. found that addition of acids, or monovalent ions, containing salts destabilized the GO colloids, and the aggregation was mainly caused by face-to-face interactions, whereas the addition of divalent cations containing salts caused edge-to-edge interactions during aggregation. The stability of GO colloids was found to be high in bases, and no aggregation was observed up a pH of 12.[31] In summary, even though the aggregation of colloids, in the presence of electrolytes, appears to be more or less a universal phenomenon, the above examples demonstrate that the aggregation mechanisms vary from one material to another.

In our previous work, we showed that the addition of HCl, or alkali metal hydroxides, such as NaOH, not just resulted in the flocculation of $Ti_3C_2T_z$ colloid suspensions, but, as importantly, the flocculation, after drying, resulted in a mesoporous interconnected network of crumpled MXene sheets. Another important result was that the cations of the base used for flocculation intercalated between MXene sheets. This method of creating crumpled MXenes is rapid, facile, and shows significantly higher capacity as anodes in Na-ion batteries compared to vacuum-filtered films or multilayered MXene powders.[32,33] One of the motivations for this work was to try and understand the aggregation mechanisms that lead to complete flocculation. To that effect, we systematically studied the stabilities of $Ti_3C_2T_z$ colloidal suspensions at various pHs and NaCl concentrations.

2. MATERIALS AND METHODS

2.1. Sample Preparation. The Ti_3AlC_2 powders were synthesized by mixing titanium carbide (Alfa Aesar, 99.5%, 2 μm), aluminum (Alfa Aesar, 99.5%, 325 mesh), and titanium (Alfa Aesar, 99.5%, 325 mesh) powders in a molar ratio of 2:1.05:1, respectively. The mixed powders were ball milled at 100 rpm for 24 h and then heated under argon (Ar) flow at 1350 °C for 2 h. The heating and cooling rates were set at 5 °C/min. The resulting loosely sintered blocks were ground using a milling bit on a drill press. The milled powders were passed through a 400-mesh (particle size < 38 μm) sieve for further experiments.

The Ti_3AlC_2 powder was etched in a LiF and HCl solution. First, 1 g of LiF (Alfa Aesar, 99.5%, 325 mesh) was dissolved in 10 mL of 12 M HCl (Fisher Scientific), after which 1 g of the Ti_3AlC_2 powder was slowly added to the solution. The latter was stirred for 24 h at 35 °C and 300 rpm. The slurry was later transferred into a 50 mL centrifuge tube, and deionized (DI) water was added to completely fill the remaining volume. It was then centrifuged at 3500 rpm/2300 rcf for 2 min, and the resulting clear supernatant was discarded. This washing was repeated several times until the pH of the solution was ≈7, at which point deionized (DI) water was added to the resulting $Ti_3C_2T_x$ "clay" and the mixture sonicated under bubbling Ar flow for 1 h. To avoid oxidation, the bath temperature was kept below 20 °C using ice. The solution was then centrifuged for 1 h at 5000 rpm/4700 rcf, and the supernatant was pipetted off for further use. The solid content of the supernatant was determined by vacuum filtering a known solution volume and measuring the weight of the resulting free-standing MXene film upon drying in a vacuum oven at 100 °C overnight. These films will henceforth be referred to as filtered films.

For all electrophoretic measurements, the colloidal suspension was diluted with DI water to a concentration of ≈1 mg/mL, while maintaining a pH of ≈7. To study the sedimentation characteristics, the pH was slowly reduced by adding drops of 1 M HCl or slowly increased by adding drops of 1 M NaOH (Aldrich, 97 wt %), or in the case of salts, a 0.2 M NaCl (Aldrich, >99%) solution was used.

To obtain X-ray diffraction (XRD) patterns of the powders, image them in the SEM and carry out electron-dispersive spectroscopy (EDS) analysis the excess NaOH and HCl from the sedimented MXene powder were removed as follows: the powders were first washed five times with DI water, followed by five washes with ethanol (EtOH) and then left overnight in vacuum and stored for further analysis. The samples treated with NaOH will henceforth be referred to as NaOH−$Ti_3C_2T_z$ and those treated with HCl as HCl−$Ti_3C_2T_z$.

In another set of experiments, an aqueous 0.5 M NaCl solution was prepared and added to the colloid suspension until all the flakes flocculated and later sedimented at the bottom. This was followed by a centrifugation for 10 min at 5000 rpm/4700 rcf to collect the sediments. After centrifuging, the clear supernatant was discarded and 40 mL of 200 proof EtOH was added to the centrifuge tube, and the mixture was thoroughly shaken for 5 min. This was followed by a centrifugation at 5000 rpm/4700 rcf for 10 min, and again the clear supernatant was discarded. This EtOH washing step was

DOI: 10.1021/acs.jpcc.8b08860
J. Phys. Chem. C 2018, 122, 27745−27753

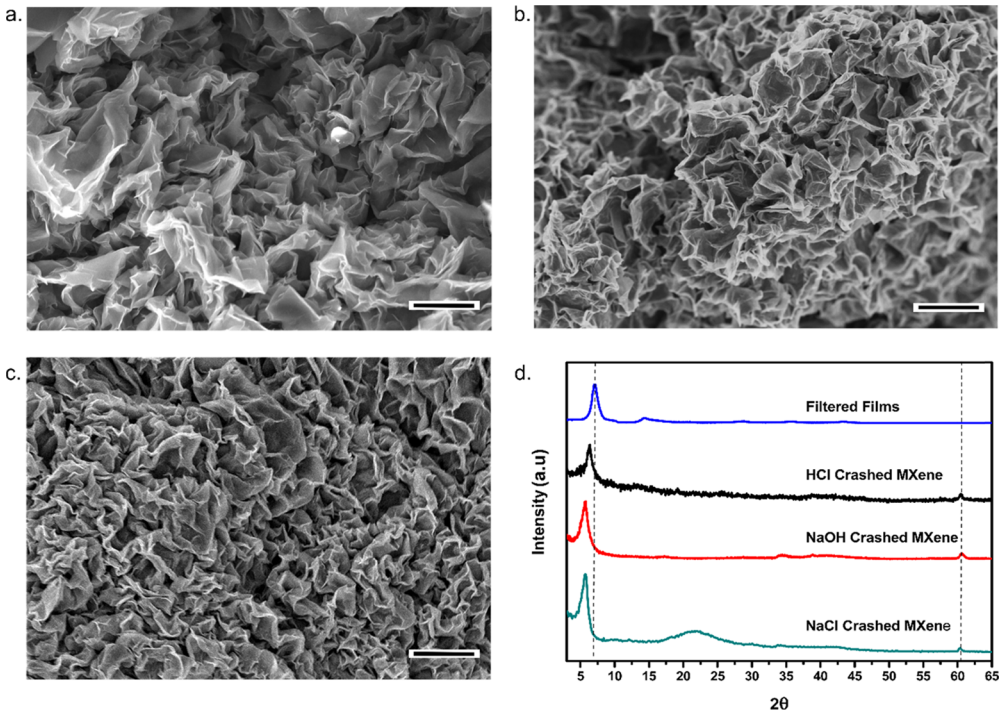

Figure 1. SEM micrographs of (a) HCl−$Ti_3C_2T_z$, (b) NaOH−$Ti_3C_2T_z$, and (c) NaCl−$Ti_3C_2T_z$ crumpled powders. Scale bar = 5 μm. (d) XRD patterns of filtered films (blue, top), HCl−$Ti_3C_2T_z$ (black, second from top), NaOH−$Ti_3C_2T_z$ (red, second from bottom), and NaCl−$Ti_3C_2T_z$ (green, bottom) samples.

repeated 10 more times (along with 5 min of shaking in the added EtOH between every wash), after which the sedimented powders were vacuum-dried overnight and stored for further characterization. The samples treated with NaCl will henceforth be referred to as NaCl−$Ti_3C_2T_z$.

EDS measurement showed some fluorine (−F-terminations) loss upon treatment with NaOH. To determine whether this loss was due to the formation of fluoride salts or simply due to an exchange with hydroxyls in solution, one part of the sedimented powders, obtained by the addition of NaOH, was washed with EtOH only, instead of water, and then dried. Since in general, fluoride salts have higher solubilities in water than EtOH,[34,35] the use of the latter increased the chances that any fluoride salts formed are not washed away and could thus be detected.

To try and better understand the nature of the charges present on the MXene surfaces/edges, colloidal suspensions of gold (Au) nanoparticles (NPs) were mixed with a colloidal suspension of MXenes. Here, 2 mL of negatively charged Au NP (10 nm diameter, citrate stabilized, nanoComposix, San Diego) colloidal suspension, at a concentration of 0.054 mg/mL, was added to 50 mL of a $Ti_3C_2T_z$ suspension with a concentration of 1 mg/mL at a pH of ≈7. After briefly shaking the mixture, a few drops were immediately dropped on a lacy carbon TEM grid (Cu-400 LC, Pacific Grid-Tech) and dried under vacuum. A similar experiment using the same concentration and volume of colloidal suspensions was also carried out but with positively charged Au NPs colloid (10 nm diameter, polyethylenimine functionalized, nanoComposix, San Diego).

2.2. Characterization. XRD patterns were recorded using a diffractometer (Rigaku Smart Lab, Tokyo, Japan) using Cu Kα radiation (40 kV and 30 mA) with a step size of 0.02° and a dwell time of 1 s in the 3−65° 2θ range. A SEM (Zeiss Supra 50 VP, Germany) was used to examine the morphology of the samples. EDS (Oxford Instruments, Abingdon, U.K.) was used to quantify the elements present. The accelerating voltage used was 10 kV, and five spots were randomly chosen over each sample, and the results were averaged.

To analyze the morphology and distribution of the as-dispersed Au NPs on the MXene flakes, a TEM (JEOL 2100 LaB_6, Tokyo, Japan) was used in bright-field mode with a high-resolution objective-lens pole piece (GATAN Orius SC1000 CCD camera, Pleasanton). The accelerating voltage was set to 200 kV.

A Zetasizer (nano-ZS, Malvern Panalytical, Malvern, U.K.) was used for the electrophoretic mobility measurements, and the Smoluchowski equation was used to convert the electrophoretic mobility values to zeta potentials, ς.[36] The hydrodynamic diameter, d_H, was also measured, on the same machine, using DLS. The ς-potential and size measurements were repeated three times at each pH or salt concentration and averaged. A titrator (MPT-2 Autotitrator) was used to in situ add volumes of titrant to change the pH (0.1 M HCl or 0.1 M NaOH) or salt (0.2 M NaCl) concentrations. Between each electrolyte concentration change, the mixture was allowed to equilibrate for 5 min before measuring ς and d_H.

3. RESULTS

3.1. Effects of pH. Typical SEM micrographs of the HCl−$Ti_3C_2T_z$ and NaOH−$Ti_3C_2T_z$ crumpled powders—shown in Figure 1a,b, respectively—are identical to those shown in our previous work.[32,33] Those of the NaCl−$Ti_3C_2T_z$ powders are shown in Figure 1c. The corresponding XRD patterns are shown in Figure 1d. For the filtered films, one strong peak corresponding to the 002 planes at 7.1° 2θ is observed. For the HCl−$Ti_3C_2T_z$, NaOH−$Ti_3C_2T_z$, and NaCl−$Ti_3C_2T_z$ powders, the 002 peaks are located at 6.3, 5.6, and 5.7°, respectively.

DOI: 10.1021/acs.jpcc.8b08860
J. Phys. Chem. C 2018, 122, 27745−27753

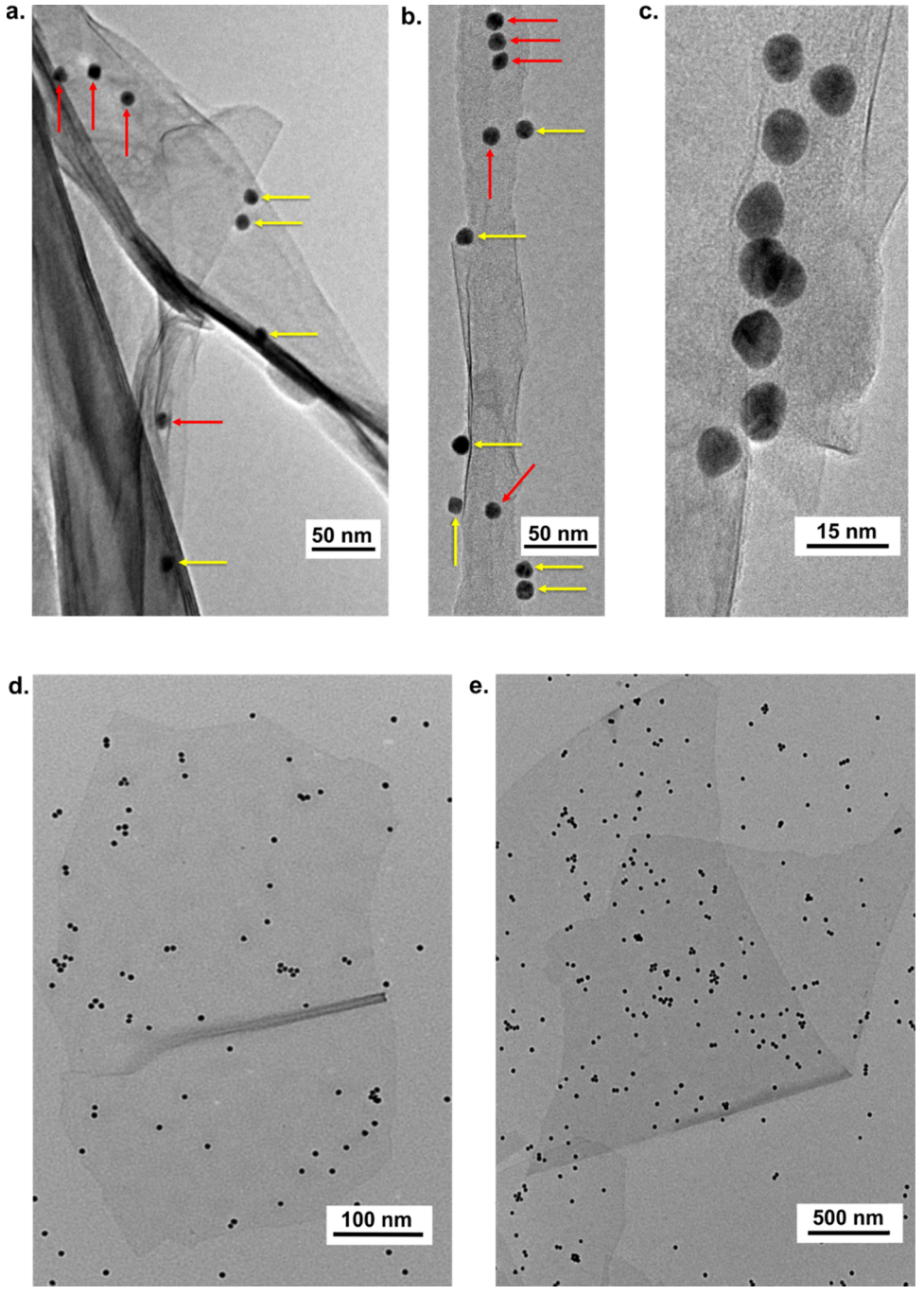

Figure 2. Typical TEM images of $Ti_3C_2T_z$ flakes decorated by Au nanoparticles. In panels (a)−(c), the gold NPs were negatively charged; in panels (d) and (e), they were positive. Yellow arrows in (a) and (b) point to NPs that are clearly on flake edges. The red arrows point to NPs that at first look appear not to be at the edges but that careful observation shows them to also be on flake edges.

Also a peak at ≈61° that corresponds to the (110) plane is observed for all patterns except in those of the filtered films.

TEM images (Figure 2a−c) of individual sheets obtained from the colloidal suspension of $Ti_3C_2T_z$ flakes and negatively charged Au NPs clearly show that the majority of the latter are aligned at, or near, the edges. The Au NPs marked by yellow arrows are clearly on, or near, the edges of the MXene sheets. And although some of the Au NPs do not at first sight appear to be located at the edges, careful observation of Figure 2a shows that indeed they are. For example, the three gold NPs marked with red arrows in the right-hand top corner are aligned near the edge of a MXene sheet lying just underneath them. The same is true for the two Au NPs in Figure 2b, again denoted by red arrows, that seem to lie directly in the middle of the sheet but are actually on the edges of MXene sheets underneath them. The alignment of Au NPs at the edges is most evident in Figure 2c. Not surprisingly, when the starting Au NPs were positive, their distribution (Figure 2d,e) was much more uniform, and quite different from, than when they were negative. In this case, a more or less uniform distribution is observed.

Figure 3a plots the dependencies of ς (left y-axis, Figure 3a) and d_H (right y-axis, Figure 3a) on pH. The fact that at pH ≈ 7, $\varsigma = -53$ mV (Figure 3a) explains why the colloid suspension is

DOI: 10.1021/acs.jpcc.8b08860
J. Phys. Chem. C 2018, 122, 27745−27753

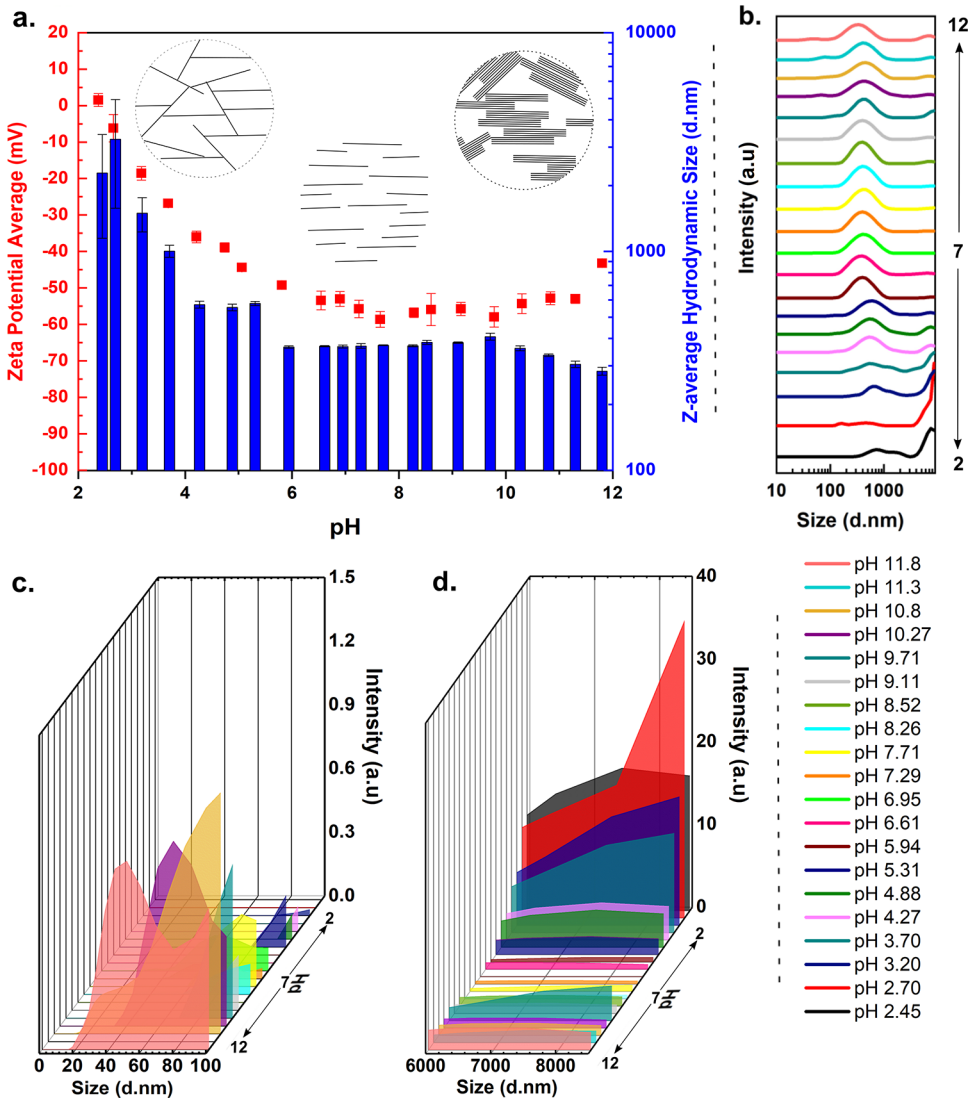

Figure 3. (a) ς-Potential (left y-axis) and average hydrodynamic size (right y-axis) vs pH. Insets show probable aggregate structures formed at low pH (left) and high pH (right), whereas complete deflocculation is represented by the middle inset. (b) Dynamic light scattered intensity vs size distribution between 10 and 9000 nm at various pH values. (c, d) Enlarged sections of (b) in the 0−100 nm size range (c) and in the 6000−9000 nm size range (d) (x-axis) vs pH (z-axis) and intensity (y-axis). Color legend shown in the bottom right corner is the same for (b)−(d). Intensity scales (y-axis) in (b)−(d) are not the same and have been adjusted for better visibility, but the intensity ratios inside each individual plot are comparable.

stable.[36] Both ς and d_H are asymmetric around neutral pH. Upon the addition of HCl, ς increases with decreasing pH ($\varsigma_{pH=7} = -53$ mV, $\varsigma_{pH=2} = 0$ mV). Upon increasing the pH, and up to a pH of ≈10, ς is more or less constant, after which it increases slightly ($\varsigma_{pH=7} = -53$ mV, $\varsigma_{pH=12} = -45$ mV).

From DLS, the average d_H was calculated to be around 500 nm at pH ≈ 7 (Figure 3a,b). This size range is in good agreement with the literature values of MXene sheets synthesized by similar methods.[8,17,37] This peak around 500 nm shifts toward higher values with decreasing pH. As importantly, new peaks start to appear at higher values (>6000 nm, Figure 3d), indicating the formation of quite large aggregates. Figure 3b also shows that an increasing number of larger aggregates (>6000 nm) start to form up to pH 10. Above pH 10, the intensity of these large aggregates starts to decrease presumably due to the settling of bigger flocs and/or disaggregation or the breaking up of larger flocks to smaller ones. This trend can also be seen from the average d_H values in Figure 3a, where the aggregate size increases slightly, up to pH 10, before it starts decreasing thereafter. With increasing pH, peaks—that are absent at pH < 7—start to appear below 100 nm (Figure 3c).

According to our EDS results (Table 1), the amounts of fluorine in the NaOH−$Ti_3C_2T_z$ powders are lower than those in the HCl−$Ti_3C_2T_z$, NaCl−$Ti_3C_2T_z$, or filtered film samples.

Table 1. EDS Results—Normalized to Three Ti Atoms—for the HCl−$Ti_3C_2T_z$, NaOH−$Ti_3C_2T_z$, and NaCl−$Ti_3C_2T_z$ Crumpled Powders and Filtered Film Samples

element	HCl−$Ti_3C_2T_z$	NaOH−$Ti_3C_2T_z$	filtered films	NaCl−$Ti_3C_2T_z$
Ti	3	3	3	3
O	1.7 ± 0.2	2.5 ± 0.1	1.5 ± 0.15	1 ± 0.15
F	1.3 ± 0.1	0.9 ± 0.05	1.5 ± 0.1	1.5 ± 0.2
Cl	0.46 ± 0	0.4 ± 0	0.4 ± 0	0.3 ± 0.05
Na		0.2 ± 0.05		0.15 ± 0.05

DOI: 10.1021/acs.jpcc.8b08860
J. Phys. Chem. C 2018, 122, 27745−27753

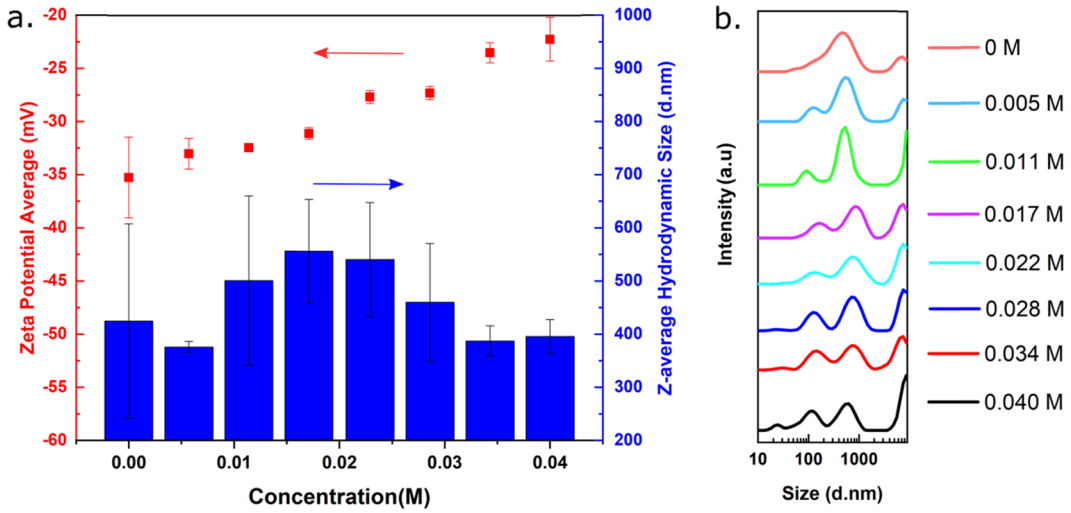

Figure 4. (a) ς-Potential (left y-axis) and average d_H (right y-axis) vs NaCl molarity. (b) Intensity of scattered light vs size distribution between 10 and 9000 nm at various NaCl salt concentration values.

The oxygen content, on the other hand, is higher in NaOH−$Ti_3C_2T_z$ powders compared to the others. Not surprisingly, the NaOH−$Ti_3C_2T_z$- and NaCl-treated samples also contained Na.

3.2. Effects of NaCl. Figure 4a plots the changes in ς (left axis) and d_H (right axis) with NaCl concentration. In this case, ς increases monotonically (ς_{0M} = −35 mV to $\varsigma_{0.04M}$ = −22 mV) with increasing electrolyte concentration, and d_H goes through a small maximum at a concentration of ≈0.02 M. As the salt was added, the pH was monitored and found not to change substantially.

Figure 4b plots the size distribution. In the absence of NaCl, the major peak is observed around 500 nm. The minor peak at ∼8000 nm is probably due to some impurities like dust or multilayer MXene stacks not removed during centrifugation. This is confirmed by the absence of such a peak in DLS data at neutral pH, as seen in Figure 3b, where the light scattering experiments were performed on an equivalent sample. It is also confirmed by TEM observations of the sample, which showed predominantly single to few layers of MXene flakes. The data in Figure 4 being from the same batch of MXene solution, we can compare the intensity ratios of peaks for evaluation of the aggregation mechanism. With increasing NaCl concentrations, a second peak starts to appear around 100−200 nm. Further, the intensity ratio of the peak at 500 nm to the peak at 100 nm decreases with increasing NaCl concentration. Meanwhile, with increasing salt concentration, the intensity ratio of the peak at 500 nm to that of 8000 nm starts to decrease, meaning that larger aggregates are forming.

4. DISCUSSION

The addition of an acid, a base, or a salt to a colloidal suspension of $Ti_3C_2T_z$ flakes induces an aggregation of the flakes that eventually leads to their sedimentation. Like in our previous work, the resulting sediment is crumpled.[32,33] Note that NaCl-induced crumpling was not reported previously. Although the MXenes, flocculated with HCl, NaOH, and NaCl, have the same morphology (Figure 1a−c), the DLS and ς measurements suggest different mechanisms for their aggregation. Before discussing the aggregation results, it is crucial to establish the charge distribution of the $Ti_3C_2T_z$ flakes at neutral pH. It is also important to note that although one of our initial goals was to understand the crumpling of the flakes, at this time why, and when, crumpling occurs is not understood. The remainder of this discussion will thus focus on the flocculation.

4.1. Charge of MXenes Flakes in Water at pH Neutral: Differences between Edges and Faces. We previously made the case that bare Ti_3C_2 blocks are positively charged because there are three Ti atoms with a +2.4 charge and only two carbon atoms with a charge of ≈−2.4.[13,38] In the simplest configuration, the latter is neutralized by OH terminations. When such flakes are placed in neutral water, deprotonation of some hydroxyl groups results in the development of negative charges on the flakes, resulting in the following equilibrium considering MXenes flakes with only OH terminations

$$Ti_3C_2(OH)_2 + zH_2O \leftrightarrow Ti_3C_2(OH)_{2-z}(O^-)_z + zH_3O^+ \quad (1)$$

The reaction is simplified in that we consider flakes with only OH terminations. In reality, the terminations include F, and a more appropriate reaction is given in the Supporting Information as reaction S1.

During etching and sonication, it is reasonable to assume that some of the Ti bonds at the edges remain unsatisfied and are thus positively charged. This is in agreement with the TEM observations: the placement of negatively charged Au NPs around the edges in Figure 2a−c and the placement of the positively charged NPs on the surface of the MXene sheets in Figure 2d,e indirectly confirm that the MXene edges are positively charged compared to the surfaces that have long been established to be negatively charged.[11,39,40] The number/concentration of negatively charged Au NPs attached to the MXene flakes' edges (7 ± 3 Au NPs/MXene sheet) (Figure 2a,c) is significantly lower than the positively charged Au NPs attached to their surfaces (300 ± 70 Au NPs/MXene sheet) (Figure 2d,e). This difference reflects the paucity of edges compared to surfaces.

4.2. Aggregation Mechanism at Low pH. With decreasing pH, the equilibrium in reaction 1 shifts toward the left, that in turn reduces ς . In kaolinite clays, the bond energy calculations carried out by Lawrence in 1958 show that clay edges preferentially adsorb OH^- ions over Cl^- ions and that in general the larger the anionic radius, the more unlikely

DOI: 10.1021/acs.jpcc.8b08860
J. Phys. Chem. C 2018, 122, 27745−27753

is its adsorption at the edges.[41,42] It was later shown experimentally that at neutral pH, no Cl^- ions absorb at the clay edges, and at low pH, the anion-exchange capacity was much lower compared to the cation-exchange capacity.[22,43,44] As in clays, we show here that the edges are positively charged at neutral pH. It is thus reasonable to assume that the same behavior is observed here: the edges remain positively charged in acidic environments as the H^+ ions do not interact with the positive edges because of Coulombic repulsion, whereas the Cl^- ions do not completely absorb on the edges due to their larger hydration radii (r_{Cl^-} = 0.175 nm) and lower electronegativity compared to the OH^- anions.[42,43]

Figure 3b,d show that large aggregates start forming around pH 4, suggesting lower stability of MXene colloids in acidic media. Even though ζ is negative up to pH 2.5, aggregation commences between pH 5 and 3, as evidenced by the fact that centrifugation in that pH range results in clear supernatants (see the Supporting Information Figure S1). This can be explained by the fact that the electrostatic repulsion helps maintain colloidal stability, whereas gravity causes sedimentation. As the flocs grow larger, the electrostatic forces are insufficient to balance the gravitational pull, which ultimately leads to complete sedimentation. A similar phenomenon is observed in clay colloids where stability is attributed not just to surface charges but to a combination of bulk and surface properties.[36]

As the pH decreases further, the electrostatic repulsion decreases, resulting mainly in edge−face interaction (Figure 3a, left inset). This is reflected in the DLS data, which shows aggregates forming with a size of 6000 nm and above (Figure 3b,d). The presence of such large aggregates is consistent with a more open structure formed as a result of edge−face interactions. It is also important to note that no signal is observed below 100 nm, indicating the lack of substantial lateral stacking in the 00*l* direction.

4.3. Aggregation Mechanism at High pH. When the pH is increased, the following, again considering only −OH terminations, reaction is postulated to occur

$$Ti_3C_2(OH)_2 + zOH^- \leftrightarrow Ti_3C_2(OH)_{2-z}(O^-)_z + zH_2O \quad (2)$$

A more detailed reaction can be found in the Supporting Information as reaction S2. If this were the only reaction occurring, then increasing the pH would have rendered the surface more negative. However, as the pH increases from 7 to 10, no significant changes in ζ are observed. It is thus reasonable to assume that the Na^+ cations adsorb onto the $Ti_3C_2T_z$ surfaces most likely at the $-O^-$ termination sites and possibly also partially onto −OH and −F sites in such a way as to maintain the ζ-potential more or less constant.

Because of their smaller size (r_{OH^-} = 0.11 nm), it is further reasonable to assume that in the high pH range, the hydroxyls neutralize the positive edges, which would reduce the probability of face-to-edge interactions. On the other hand, the face-to-face interactions (right inset Figure 3a) become more likely. This is confirmed by the appearance of new peaks below 100 nm indicating lateral stacking in the *c*-direction. The ζ-potential increase at pH > 12, might be due to passivation of all the positive edge sites by OH^- ions, after which the Na^+ ions start to reduce the Debye−Huckle screening lengths at both the edges and faces of the MXene sheets.[36]

Another phenomenon observed upon the addition of NaOH is the loss of F and a gain of O in the NaOH−$Ti_3C_2T_z$ samples compared to the filtered films, HCl−$Ti_3C_2T_z$ or NaCl−$Ti_3C_2T_z$ powders (see Table 1). The suspension sedimented by NaOH and then only washed with ethanol was characterized by XRD (Supporting Information Figure S2). NaF solubility in ethanol being lower than in water,[34,35] the presence of NaF in the XRD pattern indicates that some of the Na^+ ions react with the F-terminations to form NaF. The replacement of −F by −O terminations has been documented previously,[45,46] but, to our knowledge, the loss mechanism was not discussed. Based on our results we conclude that at least a portion reacts with Na to form NaF.

4.4. Effect of Salt on Aggregation Mechanism. What is most likely occurring in this case is that with increasing salt concentration, the Deybe−Huckle length decreases, leading eventually to flocculation. Indirect support for this conjecture is the constancy of the pH at ≈7 with NaCl additions. We believe that the aggregation mechanism here is face-to-face stacking of MXene sheets because the secondary peak—around 100 nm—formed after the addition of salt is significantly stronger than in the size distribution curves obtained at high pH (Figure 3c), indicating a higher degree of stacking in the lateral direction.

In general, our results are in agreement with the clay literature and the Derjaguin, Landau, Verwey, and Overbeek theory of colloids,[47,48] where the addition of an electrolyte can lead to the formation of an electric double layer. It is fairly well established that increasing the electrolyte's ionic strength decreases the thickness of the double layer that, in turn, reduces the repulsion between particles, ultimately leading to aggregation due to van der Waals attraction.[49]

5. CONCLUSIONS

Herein, we not only show, for the first time, that the edges of $Ti_3C_2T_z$ flakes are positively charged but that these positively charged edges are sensitive to pH. They also play a key role in the aggregation of $Ti_3C_2T_z$ colloid suspensions, especially in the 4−7 pH range.

Contrary to the common understanding that $Ti_3C_2T_z$ flakes only interact with cations, based on the results obtained herein, it is reasonable to conclude that anion adsorption at positively charged edge sites also plays an important role. This insight opens up a new avenue to selectively functionalize the edges differently from the faces to vary both properties and, as importantly, flocculation structures. Such selective functionalization has been demonstrated in other two-dimensional materials and has shown promise in applications as diverse as polymer composites,[50,51] sensor,[52] bioluminescent markers,[53] optoelectronics,[54,55] and so on.

Understanding the flocculation and deflocculation mechanisms of clay colloids helps in their transport over relatively long distances during industrial processing. Deflocculated suspensions are readily transported via pipelines, and then—by the simple addition of a salt, acid, or base depending on the ultimate application—the clay particles can be easily separated from water.[56] Since there is no reason to believe that MXene flakes will act differently, it follows that in addition to their scientific merit, the results obtained herein may prove important for scaling up MXene production in the future.

Lastly, a running theme in some of our recent work on MXenes is their similarities with some clays.[8,21,57] There are however fundamental differences between the two. Probably the most fundamental is how charge develops. In clays, the charge results from the replacement of Si^{4+} with aliovalent

DOI: 10.1021/acs.jpcc.8b08860
J. Phys. Chem. C 2018, 122, 27745−27753

cations, most commonly Al^{3+}. It follows that the surface charges in clays depend on their composition.[28] In MXenes in general, and $Ti_3C_2T_z$ in particular, the charge develops because of an imbalance between the charges on the Ti and C atoms in the Ti_3C_2 blocks.[13,34] In other words, the charges are intrinsic to the material, which, in turn, should result in much more reproducibility between various studies. It also implies that the results obtained herein should be of general validity for, most if not, all MXenes.

■ ASSOCIATED CONTENT

Supporting Information

The Supporting Information is available free of charge on the ACS Publications website at DOI: 10.1021/acs.jpcc.8b08860.

Sedimented MXene at various electrolyte concentrations, XRD of NaOH−$Ti_3C_2T_z$ powder samples washed only with EtOH, detailed chemical reactions (PDF)

■ AUTHOR INFORMATION

Corresponding Author

*E-mail: barsoumw@drexel.edu.

ORCID

Michel W. Barsoum: 0000-0001-7800-3517

Notes

The authors declare no competing financial interest.

■ ACKNOWLEDGMENTS

This work was funded by NSF (DMR-1740795). The authors thank Dr. Yury Gogotsi and Kathleen Maleski of Drexel University for help with the zeta potential measurements. The authors also thank Sankalp Kota and Cooper Voigt for useful discussions.

■ REFERENCES

(1) Naguib, M.; Kurtoglu, M.; Presser, V.; Lu, J.; Niu, J.; Heon, M.; Hultman, L.; Gogotsi, Y.; Barsoum, M. W. Two-Dimensional Nanocrystals Produced by Exfoliation of Ti_3AlC_2. *Adv. Mater.* **2011**, *23*, 4248−4253.

(2) Tao, Q.; Dahlqvist, M.; Lu, J.; Kota, S.; Meshkian, R.; Halim, J.; Palisaitis, J.; Hultman, L.; Barsoum, M. W.; Persson, P. O. Å.; et al. Two-Dimensional $Mo_{1.33}C$ MXene with Divacancy Ordering Prepared from Parent 3D Laminate with in-Plane Chemical Ordering. *Nat. Commun.* **2017**, *8*, No. 14949.

(3) Anasori, B.; Xie, Y.; Beidaghi, M.; Lu, J.; Hosler, B. C.; Hultman, L.; Kent, P. R. C.; Gogotsi, Y.; Barsoum, M. W. Two-Dimensional, Ordered, Double Transition Metals Carbides (MXenes). *ACS Nano* **2015**, *9*, 9507−9516.

(4) Naguib, M.; Mashtalir, O.; Carle, J.; Presser, V.; Lu, J.; Hultman, L.; Gogotsi, Y.; Barsoum, M. W. Two-Dimensional Transition Metal Carbides. *ACS Nano* **2012**, *6*, 1322−1331.

(5) Halim, J.; Kota, S.; Lukatskaya, M. R.; Naguib, M.; Zhao, M.-Q.; Moon, E. J.; Pitock, J.; Nanda, J.; May, S. J.; Gogotsi, Y.; et al. Synthesis and Characterization of 2D Molybdenum Carbide (MXene). *Adv. Funct. Mater.* **2016**, *26*, 3118−3127.

(6) Zhou, J.; Zha, X.; Chen, F. Y.; Ye, Q.; Eklund, P.; Du, S.; Huang, Q. A Two-Dimensional Zirconium Carbide by Selective Etching of Al_3C_3 from Nanolaminated $Zr_3Al_3C_5$. *Angew. Chem.* **2016**, *128*, 5092−5097.

(7) Zhou, J.; Zha, X.; Zhou, X.; Chen, F.; Gao, G.; Wang, S.; Shen, C.; Chen, T.; Zhi, C.; Eklund, P.; et al. Synthesis and Electrochemical Properties of Two-Dimensional Hafnium Carbide. *ACS Nano* **2017**, *11*, 3841−3850.

(8) Ghidiu, M.; Lukatskaya, M. R.; Zhao, M.-Q.; Gogotsi, Y.; Barsoum, M. W. Conductive Two-Dimensional Titanium Carbide 'Clay' with High Volumetric Capacitance. *Nature* **2014**, 78−81.

(9) Novoselov, K. S.; et al. Electric Field Effect in Atomically Thin Carbon Films. *Science* **2004**, *306*, 666−669.

(10) Mashtalir, O.; Naguib, M.; Mochalin, V. N.; Dall'Agnese, Y.; Heon, M.; Barsoum, M. W.; Gogotsi, Y. Intercalation and Delamination of Layered Carbides and Carbonitrides. *Nat. Commun.* **2013**, *4*, No. 1716.

(11) Naguib, M.; Unocic, R. R.; Armstrong, B. L.; Nanda, J. Large-Scale Delamination of Multi-Layers Transition Metal Carbides and Carbonitrides "MXenes.". *Dalton Trans.* **2015**, *44*, 9353−9358.

(12) Persson, I.; Näslund, L.-Å.; Halim, J.; Barsoum, M. W.; Darakchieva, V.; Palisaitis, J.; Rosen, J.; Persson, P. O. Å. On the Organization and Thermal Behavior of Functional Groups on Ti_3C_2 MXene Surfaces in Vacuum. *2D Mater.* **2018**, *5*, No. 015002.

(13) Halim, J.; Cook, K. M.; Naguib, M.; Eklund, P.; Gogotsi, Y.; Rosen, J.; Barsoum, M. W. X-Ray Photoelectron Spectroscopy of Select Multi-Layered Transition Metal Carbides (MXenes). *Appl. Surf. Sci.* **2016**, *362*, 406−417.

(14) Harris, K. J.; Bugnet, M.; Naguib, M.; Barsoum, M. W.; Goward, G. R. Direct Measurement of Surface Termination Groups and Their Connectivity in the 2D MXene V_2CT_x Using NMR Spectroscopy. *J. Phys. Chem. C* **2015**, *119*, 13713−13720.

(15) Hope, M. A.; Forse, A. C.; Griffith, K. J.; Lukatskaya, M. R.; Ghidiu, M.; Gogotsi, Y.; Grey, C. P. NMR Reveals the Surface Functionalisation of Ti_3C_2 MXene. *Phys. Chem. Chem. Phys.* **2016**, *18*, 5099−5102.

(16) Maleski, K.; Mochalin, V. N.; Gogotsi, Y. Dispersions of Two-Dimensional Titanium Carbide MXene in Organic Solvents. *Chem. Mater.* **2017**, *29*, 1632−1640.

(17) Maleski, K.; Ren, C. E.; Zhao, M.-Q.; Anasori, B.; Gogotsi, Y. Size-Dependent Physical and Electrochemical Properties of Two-Dimensional MXene Flakes. *ACS Appl. Mater. Interfaces* **2018**, *10*, 24491−24498.

(18) Akuzum, B.; Maleski, K.; Anasori, B.; Lelyukh, P.; Alvarez, N. J.; Kumbur, E. C.; Gogotsi, Y. Rheological Characteristics of 2D Titanium Carbide (MXene) Dispersions: A Guide for Processing MXenes. *ACS Nano* **2018**, *12*, 2685−2694.

(19) Alhabeb, M.; Maleski, K.; Mathis, T. S.; Sarycheva, A.; Hatter, C. B.; Uzun, S.; Levitt, A.; Gogotsi, Y. Selective Etching of Silicon from Ti_3SiC_2 (MAX) To Obtain 2D Titanium Carbide (MXene). *Angew. Chem., Int. Ed.* **2018**, *57*, 5444−5448.

(20) Ying, Y.; Liu, Y.; Wang, X.; Mao, Y.; Cao, W.; Hu, P.; Peng, X. Two-Dimensional Titanium Carbide for Efficiently Reductive Removal of Highly Toxic Chromium(VI) from Water. *ACS Appl. Mater. Interfaces* **2015**, *7*, 1795−1803.

(21) Ghidiu, M.; Halim, J.; Kota, S.; Bish, D.; Gogotsi, Y.; Barsoum, M. W. Ion-Exchange and Cation Solvation Reactions in Ti_3C_2 MXene. *Chem. Mater.* **2016**, *28*, 3507−3514.

(22) Ras, R. H. A.; Umemura, Y.; Johnston, C. T.; Yamagishi, A.; Schoonheydt, R. A. Ultrathin Hybrid Films of Clay Minerals. *Phys. Chem. Chem. Phys.* **2007**, *9*, 918−932.

(23) Schofield, R. K.; Samson, H. R. Flocculation of Kaolinite Due to the Attraction of Oppositely Charged Crystal Faces. *Discuss. Faraday Soc.* **1954**, *18*, 135.

(24) Thießen, P. A. Kennzeichnung Submikroskopischer Grenzflächenbereiche Verschiedenartiger Wirksamkeit. *Z. Anorg. Chem.* **1947**, *253*, 161−169.

(25) Rand, B.; Pekenć, E.; Goodwin, J. W.; Smith, R. W. Investigation into the Existence of Edge—face Coagulated Structures in Na-Montmorillonite Suspensions. *J. Chem. Soc., Faraday Trans. 1* **1980**, *76*, 225.

(26) Pecini, E. M.; Avena, M. J. Measuring the Isoelectric Point of the Edges of Clay Mineral Particles: The Case of Montmorillonite. *Langmuir* **2013**, *29*, 14926−14934.

(27) Wang, J.; Wheeler, P. A.; Jarrett, W. L.; Mathias, L. J. Synthesis and Characterization of Dual-Functionalized Laponite Clay for Acrylic Nanocomposites. *J. Appl. Polym. Sci.* **2007**, *106*, 1496−1506.

DOI: 10.1021/acs.jpcc.8b08860
J. Phys. Chem. C 2018, 122, 27745−27753

(28) Swartzen-Allen, S. L.; Matijevic, E. Surface and Colloid Chemistry of Clays. *Chem. Rev.* **1974**, *74*, 385−400.
(29) Pavlovic, M.; Huber, R.; Adok-Sipiczki, M.; Nardin, C.; Szilagyi, I. Ion Specific Effects on the Stability of Layered Double Hydroxide Colloids. *Soft Matter* **2016**, *12*, 4024−4033.
(30) Rouster, P.; Pavlovic, M.; Szilagyi, I. Destabilization of Titania Nanosheet Suspensions by Inorganic Salts: Hofmeister Series and Schulze-Hardy Rule. *J. Phys. Chem. B* **2017**, *121*, 6749−6758.
(31) Wu, L.; Liu, L.; Gao, B.; Muñoz-Carpena, R.; Zhang, M.; Chen, H.; Zhou, Z.; Wang, H. Aggregation Kinetics of Graphene Oxides in Aqueous Solutions: Experiments, Mechanisms, and Modeling. *Langmuir* **2013**, *29*, 15174−15181.
(32) Natu, V.; Clites, M.; Pomerantseva, E.; Barsoum, M. W. Mesoporous MXene Powders Synthesized by Acid Induced Crumpling and Their Use as Na-Ion Battery Anodes. *Mater. Res. Lett.* **2018**, *6*, 230−235.
(33) Zhao, D.; Clites, M.; Ying, G.; Kota, S.; Wang, J.; Natu, V.; Wang, X.; Pomerantseva, E.; Cao, M.; Barsoum, M. W. Alkali-Induced Crumpling of $Ti_3C_2T_x$ (MXene) to Form 3D Porous Networks for Sodium Ion Storage. *Chem. Commun.* **2018**, 4533−4536.
(34) Germuth, F. G. The Solubilities of Alkali Bromides and Fluorides in Anhydrous Methanol, Ethanol, and Butanol. *J. Franklin Inst.* **1931**, *212*, 343−349.
(35) Reynolds, J. G.; Belsher, J. D. A Review of Sodium Fluoride Solubility in Water. *J. Chem. Eng. Data* **2017**, *62*, 1743−1748.
(36) Sennett, P.; Olivier, J. P. Colloidal Dispersions, Electrokinetic Effects, and the Concept of Zeta Potential. *Ind. Eng. Chem.* **1965**, *57*, 32−50.
(37) Anasori, B.; Lukatskaya, M. R.; Gogotsi, Y. 2D Metal Carbides and Nitrides (MXenes) for Energy Storage. *Nat. Rev. Mater.* **2017**, *2*, No. 16098.
(38) Lukatskaya, M. R.; Bak, S.-M.; Yu, X.; Yang, X.-Q.; Barsoum, M. W.; Gogotsi, Y. Probing the Mechanism of High Capacitance in 2D Titanium Carbide Using In Situ X-Ray Absorption Spectroscopy. *Adv. Energy Mater.* **2015**, *5*, No. 1500589.
(39) Collini, P.; Kota, S.; Dillon, A. D.; Barsoum, M. W.; Fafarman, A. T. Electrophoretic Deposition of Two-Dimensional Titanium Carbide (MXene) Thick Films. *J. Electrochem. Soc.* **2017**, *164*, D573−D580.
(40) Xie, X.; Zhao, M.-Q.; Anasori, B.; Maleski, K.; Ren, C. E.; Li, J.; Byles, B. W.; Pomerantseva, E.; Wang, G.; Gogotsi, Y. Porous Heterostructured MXene/Carbon Nanotube Composite Paper with High Volumetric Capacity for Sodium-Based Energy Storage Devices. *Nano Energy* **2016**, *26*, 513−523.
(41) Lawrence, W. G. Theory of Ion Exchange and Development of Charge in Kaolinite-Water Systems. *J. Am. Ceram. Soc.* **1958**, *41*, 136−140.
(42) Marcus, Y. Ionic Radii in Aqueous Solutions. *Chem. Rev.* **1988**, *88*, 1475−1498.
(43) Bergaya, F.; Lagaly, G.; Vayer, M. *Handbook of Clay Science*; Bergaya, F., Theng, B. K. G., Lagaly, G., Eds.; Elsevier, 2006; Volume 1, pp 1−1224.
(44) Ferris, A.; Jepson, W. The Exchange Capacities of Kaolinite and the Preparation of Homoionic Clays. *J. Colloid Interface Sci.* **1975**, *51*, 245−259.
(45) Lian, P.; Dong, Y.; Wu, Z.-S.; Zheng, S.; Wang, X.; Wang, S.; Sun, C.; Qin, J.; Shi, X.; Bao, X. Alkalized Ti_3C_2 MXene Nanoribbons with Expanded Interlayer Spacing for High-Capacity Sodium and Potassium Ion Batteries. *Nano Energy* **2017**, *40*, 1−8.
(46) Dall'Agnese, Y.; Lukatskaya, M. R.; Cook, K. M.; Taberna, P.-L.; Gogotsi, Y.; Simon, P. High Capacitance of Surface-Modified 2D Titanium Carbide in Acidic Electrolyte. *Electrochem. commun.* **2014**, *48*, 118−122.
(47) Verwey, E. J. W. Theory of the Stability of Lyophobic Colloids. *J. Phys. Colloid Chem.* **1947**, *51*, 631−636.
(48) Derjaguin, B.; Landau, L. Theory of the Stability of Strongly Charged Lyophobic Sols and of the Adhesion of Strongly Charged Particles in Solutions of Electrolytes. *Prog. Surf. Sci.* **1993**, *43*, 30−59.
(49) Missana, T.; Adell, A. On the Applicability of DLVO Theory to the Prediction of Clay Colloids Stability. *J. Colloid Interface Sci.* **2000**, *230*, 150−156.
(50) Wang, J.; Wheeler, P. A.; Jarrett, W. L.; Mathias, L. J. Synthesis and Characterization of Dual-Functionalized Laponite Clay for Acrylic Nanocomposites. *J. Appl. Polym. Sci.* **2007**, *106*, 1496−1506.
(51) Nadiv, R.; Shtein, M.; Buzaglo, M.; Peretz-Damari, S.; Kovalchuk, A.; Wang, T.; Tour, J. M.; Regev, O. Graphene Nanoribbon − Polymer Composites: The Critical Role of Edge Functionalization. *Carbon* **2016**, *99*, 444−450.
(52) Gao, J.; Liu, M.; Song, H.; Zhang, S.; Qian, Y.; Li, A. Highly-Sensitive Electrocatalytic Determination for Toxic Phenols Based on Coupled CMWCNT/Cyclodextrin Edge-Functionalized Graphene Composite. *J. Hazard. Mater.* **2016**, *318*, 99−108.
(53) Kaup, G.; Felbeck, T.; Staniford, M.; Kynast, U. Towards the Rare Earth Functionalization of Nano-Clays with Luminescent Reporters for Biophotonics. *J. Lumin.* **2016**, *169*, 581−586.
(54) Grayfer, E. D.; Kozlova, M. N.; Fedorov, V. E. Colloidal 2D Nanosheets of MoS_2 and Other Transition Metal Dichalcogenides through Liquid-Phase Exfoliation. *Adv. Colloid Interface Sci.* **2017**, *245*, 40−61.
(55) Jeong, M.; Kim, S.; Ju, S.-Y. Preparation and Characterization of a Covalent Edge-Functionalized Lipoic Acid−MoS_2 Conjugate. *RSC Adv.* **2016**, *6*, 36248−36255.
(56) Michaels, A. S.; Bolger, J. C. Settling Rates and Sediment Volumes of Flocculated Kaolin Suspensions. *Ind. Eng. Chem. Fundam.* **1962**, *1*, 24−33.
(57) Ghidiu, M.; Kota, S.; Drozd, V.; Barsoum, M. W. Pressure-Induced Shear and Interlayer Expansion in Ti_3C_2 MXene in the Presence of Water. *Sci. Adv.* **2018**, *4*, No. eaao6850.

DOI: 10.1021/acs.jpcc.8b08860
J. Phys. Chem. C 2018, 122, 27745−27753